CHARACTERISTICS OF HIGH FREQUENCY TURBULENCE DURING EDGE LOCALIZED MODES IN THE HL-2A TOKAMAK

 1,2 G.Q. Xue, 3 X.L. Zou, 2 *W.L. Zhong, 1 *Z.X. Wang, 2 R. Ke, 2 Z.C. Yang, 2 N. Wu, 2 X.X. He, 2 Y.R. Zhu, 2 A.S. Liang, 2 G.L. Xiao, 2 M. Jiang and 2 HL-2A team

¹School of Physics, Dalian University of Technology, Dalian, China

Email: zhongwl@swip.ac.cn and zxwang@dlut.edu.cn

Abstract

On the HL-2A tokamak, characteristics of high-frequency turbulence (HFT, f = 100-150 kHz) during edge-localized modes (ELMs) have been investigated. A significant delay between the onset of low-frequency turbulence (LFT, f = 20-60 kHz) and HFT is observed in small ELM crash phase. The HFT exhibits clear electromagnetic features and propagates in the ion diamagnetic drift direction with a normalized poloidal wavenumber $k_{\theta}\rho_{s} \sim 0.07$. The HFT could be Alfvén turbulence driven by fast-ion redistribution induced by ELMs since the HFT frequency is located inside the TAE frequency gap. Additionally, the delay time is found to be negatively correlated with the ELM-induced energy loss. Longer delays are associated with reduced turbulent transport and more rapid pedestal recovery, indicating a crucial role for HFT in governing edge transport dynamics and pedestal evolution during ELM events.

1. INTRODUCTION

The high-confinement mode (H-mode), first discovered in ASDEX in 1982 [1], has become the optimized operating regime for ITER and future fusion reactors due to its ability to sustain steep edge pressure gradients and reduce turbulent transport through the formation of an edge transport barrier (ETB). However, H mode is typically accompanied by edge-localized modes (ELMs) [2], transient instabilities that periodically eject energy and particles toward the plasma-facing components (PFCs) [3]. Developing robust ELM control strategies is critical for advancing magnetic confinement fusion devices. On the one hand, small-ELM or ELM-free regimes—such as quiescent H-mode [4], EDA H-mode [5], QCE H-mode [6] and I-mode [7]—have been explored in various tokamak experiments. On the other hand, external actuators have been employed to control ELM frequency and mitigate energy loss, including resonance magnetic perturbations (RMP) [8], pellet pacing [9], low Z impurity injection [10], supersonic molecular beam injection (SMBI) [11] and RF heating [11]. These efforts have achieved partial success in suppressing or mitigating ELMs, but often at the cost of added complexity or confinement degradation.

Theory and numerical simulations show that ELMs arise from a coupled peeling-ballooning modes driven by the current and pressure gradients in the pedestal region [13]. BOUT++ linear simulations reveal that the unstable mode spectrum extends over a broad range of toroidal mode numbers from low-n (n = 10–15) peeling-ballooning modes up to high-n (n = 40–80) drift–Alfvén instabilities during ELM crash [14]. It is well established that ELMs are predominantly turbulent phenomena, with turbulence levels significantly higher than those observed in ELM-free H-mode [15]. Understanding ELMs dynamics is an important issue for future fusion reactors. Exploring the characteristics of plasma turbulence during ELM crashes could provide new insights on the underlying dynamic mechanisms of transport during ELM bursts.

Experiments on various tokamaks have revealed a wide diversity in ELM precursor and post-cursor phenomena, depending on the type of ELM. For example, in ASDEX Upgrade, high-frequency magnetic perturbation precursors to type-I ELMs have been linked to saturation in the edge pressure gradient before ELM onset [2]. In JT-60U, the precursors in density fluctuations have allowed classification of ELM events into four sequential phases: precursor, collapse, recovery, and relaxation [16]. Furthermore, a post-cursor mode with many harmonic frequencies is called "palm tree mode" triggered by type I ELM in JET. The palm tree mode exhibits tearing mode structure, which could be attributed to remnants of magnetic islands generated by ergodization during the ELM [17]. In contrast, a different post-cursor mode was observed in EAST following small ELMs – a post-cursor mode propagating in the electron diamagnetic drift direction, which was modulated by a low-frequency MHD mode [18]. In DIII-D, an ELM coherent mode with a frequency of 85-105kHz during type III

²Southwestern Institute of Physics, Chengdu, China

³CEA, IRFM, Saint-Paul-Lez-Durance, France

ELMs has been considered a resistive MHD mode [19]. While much of the research has focused on the onset of ELMs, fluctuations occurring during the ELM event itself have received comparatively less attention, in part due to the very short duration of the ELM crash (usually only a few microseconds). Particularly, the underlying mechanism of turbulence influence on particle transport during ELM remains unclear.

In this paper, we report observations of a high-frequency turbulence during ELM events in the HL-2A tokamak. We characterize its temporal evolution and correlation properties. The observed turbulent fluctuations have characteristics consistent with Alfvénic turbulence, and our results suggest that the turbulence plays a role in the pedestal transport.

2. EXPERIMENTAL SETUP

The experiments reported in this study were performed in the HL-2A tokamak, which has a major radius R = 1.65 m and a minor radius a = 0.4 m. The ELMy H-mode plasmas were operated in a lower single null divertor configuration, with the ion $B \times \nabla B$ drift directed toward the X-point. Typical plasma parameters presented in this paper include a toroidal magnetic field $B_T \approx 1.3 T$, a plasma current Ip = 150 kA, and a central line-averaged electron density ne = $1.5 \sim 2.5 \times 10^{19} \text{m}^{-3}$. The auxiliary heating was provided by neutral beam injection (NBI), electron cyclotron resonance heating (ECRH), and lower hybrid wave (LHW) heating. In this work, the plasma line-averaged electron density is obtained using a far-infrared laser interferometer [20]. The radial profile of the electron density is measured by microwave reflectometry [21]. Ion temperature measurements are performed using charge exchanged recombination spectroscopy (CXRS) [22]. The density fluctuations are measured by the Beam Emission Spectroscopy (BES) diagnostic system [23,24]. The BES diagnostic detects fluorescence emitted by injected neutral beam that are collisionally excited through interactions with plasma particles. Fluctuations in the light emission intensity are related to the local density fluctuations. Thus, the local density fluctuation can be estimated by

$$\frac{\tilde{I}}{I} = C \frac{\tilde{n}_e}{n_e},\tag{1}$$

 $\frac{\tilde{I}}{I} = C \frac{\tilde{n}_e}{n_e}, \tag{1}$ where $\frac{\tilde{I}}{I}$ is the relative light intensity fluctuations, $\frac{\tilde{n}_e}{n_e}$ is the normalized electron density fluctuations, C is a coefficient that depends on local plasma parameters, including electron density, temperature, beam energy and effective charge Z_{eff} [25]. A BES diagnostic has been implemented on the HL-2A tokamak to investigate local electron density fluctuations[26]. The system consists of 48 spatial channels arranged in a two-dimensional grid (24 radial × 2 poloidal) at the outer midplane. This configuration enables measurements of both radial and poloidal wavenumber spectra of turbulent density fluctuations. The diagnostic operates at a sampling frequency of 2 MHz, with measurement radial position covering the edge region from r/a=0.8 to 1.1. On HL-2A, magnetic fluctuations are measured using Mirnov probes, with a sampling frequency of 1 MHz. The diagnostic system comprises a total of 28 magnetic pickup coils, including 10 toroidal coils distributed along the low field side, and 18 poloidal coils, of which 7 are positioned on the high field side and 11 on the low field side.

OBSERVATION OF A HFT DURING ELMS BURST

Figure 1 displays the time evolution of key plasma parameters in ELMy H-mode in HL-2A tokamak. The H-mode discharge is sustained with a total auxiliary heating power of 1.5 MW, including 1 MW NBI and 0.5 MW LHCD, as shown in figure 1(a). Figure 1(d) shows the D_{α} intensity, where the ELMs are clearly identified via the bursts in Dalpha emission intensity, which is a typical characteristic of H-mode operation. Corresponding to these ELM events, both the plasma line-averaged electron density (figure 1(b)) and the stored energy (figure 1(c)) exhibit periodic reductions, confirming the transient loss of energy associated with ELMs. Figure 1(e) displays the spectrogram of density fluctuation measured by BES system at the edge pedestal region. A significant increase in turbulence intensity is observed in coincidence with each ELM burst, indicating enhanced fluctuation activity during these events. The magnified views of the Dalpha signal and the associated turbulence spectrogram are provided in Figure 1(f) and (g), respectively. It can be observed from Figure 1(g) that there is a time delay between the low-frequency turbulence (LFT, 20~60 kHz) and the high-frequency turbulence (HFT,100~150 kHz) during the occurrence of an ELM. The LFT intensity increases nearly simultaneously with the onset of the ELM, whereas the HFT intensity also increases during the ELM event but with a noticeable time delay relative to the ELM burst or the low-frequency turbulence.

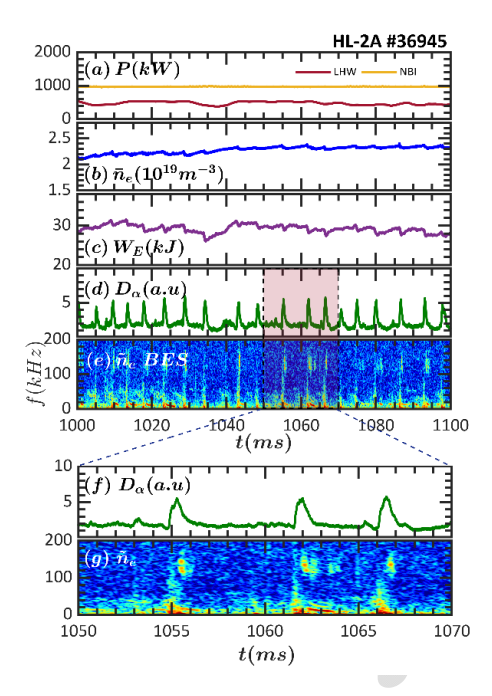


FIG. 1. Time evolutions of key parameters for H-mode plasma in the HL-2A tokamak. (a) auxiliary heating power of NBI and LHW, (b) line-averaged electron density, (c) plasma stored energy, (d) D_{α} intensity, (e) spectrogram of density fluctuation measured by BES at the pedestal region. Zoomed-in plots of (f) D_{α} intensity, (g) spectrogram of density fluctuation, respectively.

Figures 2(a1–d1) and 2(a2–d2) provide a comparative visualization of turbulence behavior during two distinct time periods characterized by large and small ELM activity, respectively. Figure 2(c1) shows the integral turbulence intensity across different frequency bands during the large ELM burst, where both HFT and LFT occur nearly simultaneously. In contrast, during the small ELM phase, a noticeable time delay is observed between the onset of LFT and HFT, with the latter lagging behind, as shown in Figure 2(c2). Figures 2(d1) and 2(d2) illustrate the temporal evolution of the pedestal electron density gradient in response to the ELM crash and subsequent recovery. Figure 2(d2) demonstrates that the maximum density gradient recovers more rapidly when a longer delay is observed in the onset of HFT. These observations suggest that high-frequency turbulence, potentially modulated by the delay time relative to LFT onset, plays a role in regulating particle transport in the pedestal region.

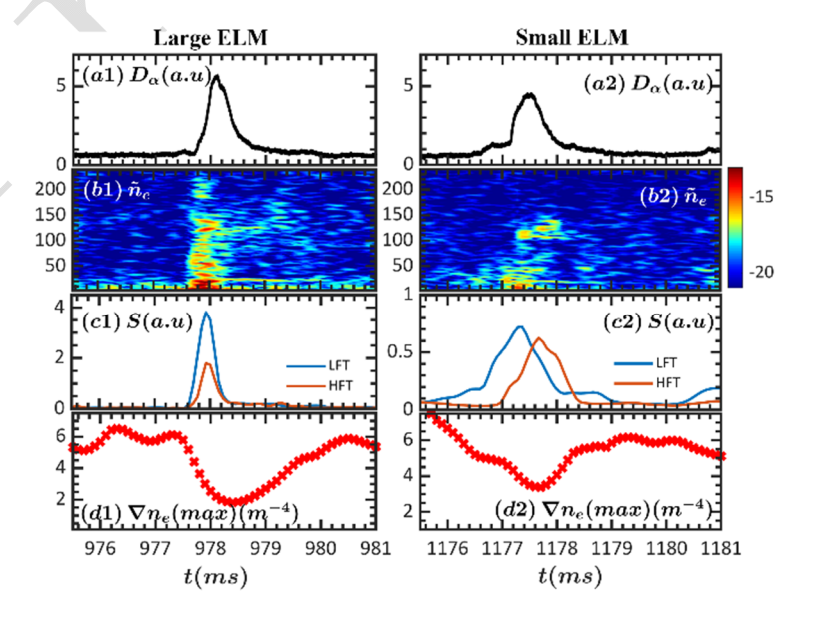


FIG. 2. Comparison of plasma edge dynamics during a large ELM (left, a1-d1) and a small ELM (right, a2-d2). (a1, a2) Dα signals, (b1, b2) spectrogram of density fluctuation, (c1, c2) integrated turbulence intensity in 20-60 kHz (blue) and 100-150 kHz (orange) bands; (d1, d2) maximum electron density gradient at pedestal region.

CHARACTERISTICS OF THE HFT

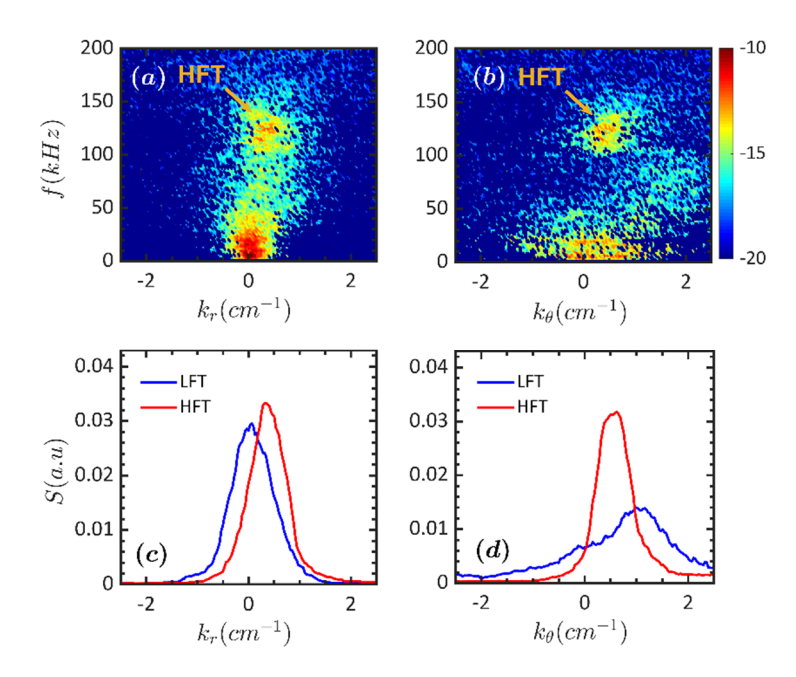


FIG. 3. (a) Radial wavenumber and (b) Poloidal wavenumber spectra of the density fluctuations at pedestal positions, (c) intensity integral of radial wavenumber in $f = 20 \sim 60$ kHz and $f = 100 \sim 160$ kHz, (d) intensity integral of poloidal wavenumber in $f = 20\sim60$ kHz and $f = 100\sim160$ kHz.

The characteristics of the HFT during ELMs are analysed using the BES 2D array, which is displaced in radial and poloidal directions at low-field side midplane. The two-point correlation method is used to estimate the local wavenumber-frequency spectrum S (k, f). This method utilizes cross-correlation between signals from different spatial channels and is based on the following approach [27]:

$$S(k,f) = \frac{1}{M} \sum_{i=1}^{M} I_{\Delta_k}[k - k_i(f)] |P_{X_1 X_2}^j(f)|, \qquad (2)$$

where M is the number of the realization divided from the fluctuations, $P_{X_1X_2}^j(f)$ is the cross-power of the density fluctuations with a separation of Δx , and the local wavenumber is given by $k_i(f) = \theta_{1,2}^i(f)/\Delta x$, $\theta_{1,2}^{i}(f)$ is the phase shift between two fluctuations in the frequency domain. The indicator function $I_{\Delta k}(x)$ is defined as

$$I_{\Delta k}(x) = \begin{cases} 1 & -\Delta k/2 \le x \le \Delta k/2 \\ 0 & elsewhere \end{cases}$$
 the local averaged wavenumber can be readily estimated: (3)

$$\langle k \geq \sum_{f} \bar{k}(f)S(f),$$
 (4)

$$\langle k \geq \sum_{f} \overline{k}(f)S(f), \tag{4}$$

$$S(k|f) = S(k,f) / \sum_{k} S(k,f), \tag{5}$$

here, S(k|f) represents the conditional wavenumber spectrum density and $\bar{k}(f) = \sum_{k} k \cdot S(k|f)$ is statistic dispersion relation.

Figure 3 (a) and 3(b) show the radial and poloidal wavenumber-frequency spectra obtained from adjacent radial and poloidal channels of the BES at the pedestal region, respectively. The BES channels are separated by 0.88 cm in the radial direction and 1.2 cm in the poloidal direction. It should be noted that the spectra were performed from concatenated BES data corresponding to 10 ELM events. This approach focuses specifically on the ELM crash phases, deliberately excluding the inter-ELM periods to emphasize the transient features associated with ELM-induced turbulence. The blue and red lines in the plots (figure 3(c) and (d)) represent wavenumber spectrum $S(k) = \sum_f S(k, f)$ integrated over the frequency bands of 20-60kHz and 100-150 kHz respectively. The HFT propagates radially outward as shown in figure 3(c), while the LFT shows no significant radial propagation. It is observed that the averaged poloidal wavenumber of the HF turbulence is about $0.4 \, \text{cm}^{-1}$, indicating that the mode propagates in the ion diamagnetic drift direction in the laboratory frame. The corresponding poloidal and toroidal mode numbers are estimated to be $m \sim 12$ and $n \sim 5$, according to the relations $m = k_{\theta} r$ and n = m/q, where r is the radial position at which the fluctuation is measured and q is the local safety factor.

Since the HFT is excited during the ELM crash phase when steep density and temperature gradients are strongly reduced, pressure-gradient-driven instabilities, such as the kinetic ballooning mode (KBM) [28], can be effectively excluded. In addition, experimental observations from ASDEX Upgrade, KSTAR, and DIII-D have consistently demonstrated that there is a strong interaction between fast ions and ELM-induced fluctuations. Simulations further indicate that energetic particles significantly modify the spatiotemporal structure of ELMs through resonant energy exchange mechanisms between fast ions and electromagnetic perturbations associated with ELMs [29,30]. In the presence of energetic particles kinetic effects, the ELM perturbation structure is radially extended, resulting in broad radial redistribution of fast ions. Similarly, in the HL-2A tokamak, strong coupling between AEs and ELM has also been experimentally confirmed [31]. In our experiments, the HFT frequency is found to be approximately located near the center of the TAE frequency gap(~118kHz), estimated using the expression [32]:

$$f_{TAEgap} = 0.13 \times 10^{13} B_T / (q \times R_m \times (n_e^{ave})^{0.5}),$$
 (6)

where B_T is the toroidal magnetic field, q is the safety factor, R_m is the major radius, and n_e^{ave} is the line-averaged electron density. Therefore, combined with theoretical and simulation analysis, the HFT may potentially be Alfvén turbulence driven by fast-ion redistribution induced by ELMs.

5. EFFECT OF THE HFT ON ELM ENERGY LOSS

Figure 4(a1) and Figure 4(a2) present the raw signals of density fluctuations measured by the BES system during a large ELM event. Specifically, Figure 4(a1) shows the LFT component filtered in the 20–60 kHz range, while Figure 4(a2) displays the HFT component filtered in the 100–150 kHz range. In both panels, the thick solid lines represent the amplitude envelopes of the respective density fluctuation signals. For comparison, Figure 4(b1) and Figure 4(b2) show the corresponding LFT and HFT components during a small ELM event, respectively, following the same frequency filtering and envelope extraction procedures. It can be observed from the amplitude envelopes that, during the large ELM event, the HFT and LFT components exhibit nearly synchronous behavior, with no evident time delay. In contrast, during the small ELM event, a clear temporal delay is observed, with the HFT lagging behind the LFT.

To further investigate the temporal relationship between HFT and LFT, cross-correlation analysis (CCF) is employed. The cross-correlation function of two signals x(t) and y(t) is defined as:

where
$$\tau$$
 is the time lag, and $\langle \cdot \rangle$ denotes ensemble averaging. The normalization ensures $\gamma_{xy}(\tau) \in \frac{\langle [x(t+\tau)-\bar{x}][y(t)-\bar{y}] \rangle}{\sqrt{\langle [x(t+\tau)-\bar{x}]^2 \rangle \langle [y(t)-\bar{y}]^2 \rangle}}$, (7)

where τ is the time lag, and $\langle \cdot \rangle$ denotes ensemble averaging. The normalization ensures $\gamma_{xy}(\tau) \in [-1,1]$, with values approaching +1 indicating strong positive correlation and values near -1 indicating anti-correlation. The time lag τ at which $\gamma_{xy}(\tau)$ reaches its maximum value corresponds to the time delay between the two signals. Figure 4(c) presents the results of the cross-correlation function (CCF) between the HFT and LFT components. The blue curve corresponds to a large ELM event, while the red curve represents a small ELM event. A positive time delay ($\Delta \tau > 0$) indicates that the LFT leads the HFT. For the large ELM case, only a small delay less than 100 μ s is observed. This indicates that both frequency components may be simultaneously excited by the strong perturbation associated with the large ELM. In contrast, during the small ELM event, a clear temporal delay is evident, with the HFT lagging behind the LFT by approximately 600 μ s. These results indicate that the time delay between the onset of HFT and LFT correlates with the ELM intensity, where weaker ELMs exhibit a more pronounced delay, while stronger ELMs tend to trigger both components nearly simultaneously.

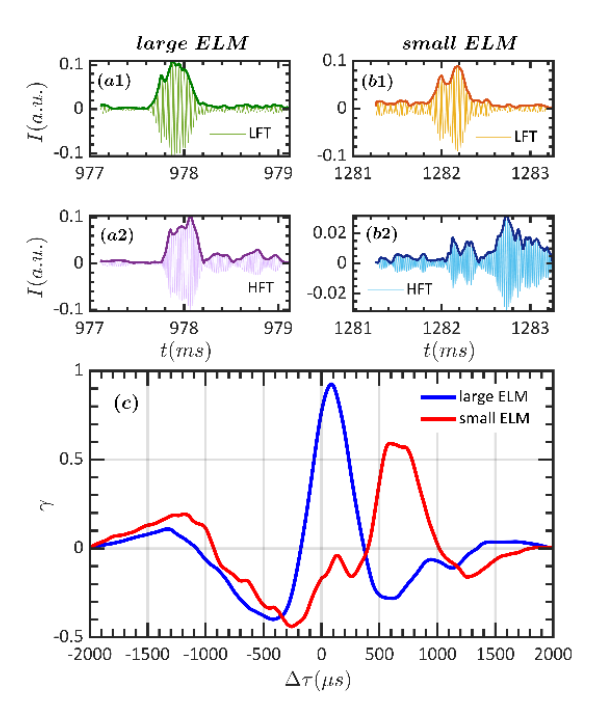


FIG. 4. Raw signals of density fluctuations measured in the frequency ranges of 20–60 kHz (a1, b1) and 100–150 kHz (a2, b2) and its envelope at $t_1 \sim 980$ ms (a) and $t_2 = 1280$ ms (b), respectively. (c) Comparison of the time delay between the HF turbulence and LF turbulence at different time.

In order to clarify the role of HFT during the ELM crash phase, figure 5 presents the correlation between the time delay ($\Delta\tau$) of LFT and HFT, and the normalized stored energy loss ($\Delta W/W$) during ELM events. Here, $\Delta W/W$ is used as a quantitative proxy for the ELM size. The data points were obtained from multiple ELMy H-mode discharges. It has been shown that greater $\Delta W/W$, that is, larger ELMs, are associated with shorter $\Delta\tau$. This suggests that longer delay times may contribute to a mitigation of ELM-induced energy losses. It can be considered that the recovery time of the plasma pedestal following an ELM crash is found to be shorter for smaller ELMs, implying that a longer delay is correlated with faster particle transport. These results suggest a possible interplay between turbulence dynamics and ELM crash behavior. In particular, the HFT appears to regulate the rate of pedestal recovery following ELM crashes via turbulent transport mechanisms. Overall, the observed inverse relationship between delay time and ELM energy loss demonstrates the potential of exploiting turbulence dynamics for reduced ELM energy losses and pedestal performance optimization.

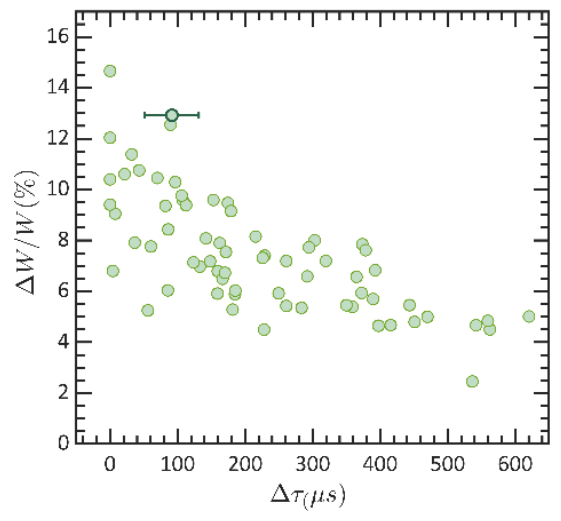


FIG. 5. Energy loss caused by ELM against the time delay of the HFT and LFT

6. SUMMARY

In summary, characteristics of high-frequency turbulence (HFT) during the ELM has been investigated in the ELMy H-mode plasmas on the HL-2A tokamak. It is interesting that there is a time delay between the lowfrequency turbulence (LFT, f = 20~60 kHz) and the high-frequency turbulence (HFT, f = 110~160 kHz) during ELM events. The experiment suggests that the HFT could be an electromagnetic instability because it exists on both density fluctuations and magnetic perturbations. The characteristics of the HF mode during ELMs are analysed using the BES system. The mode is found to propagate in the ion diamagnetic drift direction, with a poloidal wavenumber of $k_{\theta} \sim 0.4 \ cm^{-1}$. Combined with theoretical and simulation analysis, the HFT may potentially be Alfvén turbulence driven by fast-ion redistribution induced by ELMs. Bicoherence analysis reveals a nonlinear interaction between this high frequency mode and broadband background turbulence, implying that the HFT contributes to turbulent transport processes. Further investigation shows that the delay time between the HFT and LFT is correlated with the energy loss of the ELM. Notably, as the delay time increases, the energy loss per ELM decreases. Additionally, the radial correlation length of the HFT is found to shrink with increasing delay time, suggesting a reduction in turbulent transport. The recovery time of the plasma pedestal is shorter following smaller ELMs, implying that the longer delay times may be associated with faster pedestal recovery. These results support the hypothesis that high-frequency turbulence plays a significant role in regulating edge transport and pedestal dynamics during ELMs.

ACKNOWLEDGEMENTS

This work is supported by the National Natural Science Foundation of China under Grant Nos. 12435014 and U21A20440.

REFERENCES

- [1] F. Wagner et al., Phys. Rev. Lett. 49, 1408 (1982).
- [2] H. Zohm, Plasma Phys. Control. Fusion 38, 105 (1996).
- [3] G. Federici et al., Nucl. Fusion 41, 1967 (2001)
- [4] K. H. Burrell et al., Phys. Plasmas 8, 2153 (2001).
- [5] M. Greenwald et al., Phys. Plasmas 6, 1943 (1999).
- [6] M. Faitsch et al., Nucl. Mater. Energy 26, 100890 (2021).
- [7] D.G. Whyte et al., Nucl. Fusion 50, 105005 (2010).
- [8] T. E. Evans et al., Nucl. Fusion 48, 024002 (2008).
- [9] P. T. Lang et al., Phys. Rev. Lett. 79, 1487 (1997).
- [10] W. L. Zhong et al., Rev. Sci. Instrum. 85, 013507 (2014).
- [11] W. W. Xiao et al., Nucl. Fusion 54, 023003 (2014).
- [12] G. L. Xiao et al., Nucl. Fusion 59, 126033 (2019).
- [13] W. Suttrop et al., Plasma phys. Control. Fusion 42, A1 (2000).
- [14] N. Li et al., Nucl. Fusion 62, 096030 (2022).
- [15] H. Zohm et al., Nucl. Fusion 32, 489 (1992).
- [16] N. Oyama et al., Plasma Phys. Control. Fusion 43, 717 (2001).
- [17] H.R. Koslowski et al., Nucl. Fusion 45, 201 (2005).
- [18] N. Zhao et al., Plasma Sci. Technol. 20, 024007 (2018).
- [19] S. Coda et al., Nucl. Fusion 41, 1885 (2001).
- [20] Li Y.G et al., Rev. Sci. Instrum. 88 083508 (2017).
- [21] W. L. Zhong et al., Rev. Sci. Instrum. 85 013507 (2014).
- [22] D.L. Yu et al., Rev. Sci. Instrum. 85 11E402 (2014).
- [23] R. J. Fonck et al., Rev. Sci. Instrum. 61, 3487 (1990).
- [24] R. D. Durst et al., Rev. Sci. Instrum. 63, 4907 (1992).
- [25] G. R. McKee et al., Rev. Sci. Instrum. 74, 2014 (2003).
- [26] R. Ke et al., Rev. Sci. Instrum. 89, 10D122 (2018).

IAEA-CN-#3138

- [27] J. M. Beall, Y. C. Kim, and E. J. Powers J. Appl. Phys. 53, 3933 (1982).
- [28] W. M. Tang, J. W. Connor, and R. J. Hastie. Nucl. Fusion 20, 1439 (1980).
- [29] M. Garcia-Munoz et al., Nucl. Fusion 53, 123008 (2013).
- [30] A. Jansen Van Vuuren et al., Nucl. Fusion 61, 046001 (2021).
- [31] M. Jiang et al., Nucl. Fusion **62**, 076025 (2022)
- [32] M.P. Gryaznevich and S.E. Sharapov, Nucl. Fusion 46, S942 (2006).